Electronic Supplementary Material (ESI) for Journal of Materials Chemistry A.

Characterising local environments in high energy density Li-ion battery cathodes: a combined NMR and first principles study of $LiFe_xCo_{1-x}PO_4$

Fiona C. Strobridge,[a] Derek S. Middlemiss,[ag] Andrew J. Pell,[bg] Michal Leskes,[a] Raphaële J. Clément,[a] Frédérique Pourpoint,[ag] Zhouguang Lu,[c] John V. Hanna,[d] Guido Pintacuda,[b] Lyndon Emsley,[b] Ago Samoson[de] and Clare P. Grey*[af]

Electronic Supplementary Information

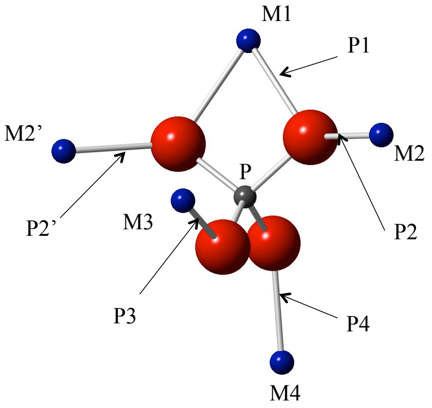

Fig. 1 The local environment of a P atom in the olivine structure, $LiMPO_4$, (M = Fe, Co). There are 5 M-O-P pathways, however 2 are equivalent (P2 and P2'), resulting in 4 distinct M-O-P pathways.

	Bond Angle		
Pathway	$LiFePO_4$	$LiCoPO_4$	Difference in Bond angles
P1	94.272°	93.892°	0.38°
P2	128.06°	127.47°	0.586°
P3	120.35°	122.87°	-2.516°
P4	123.65°	126.22°	-2.566°

Table 1 Comparison of the $LiFePO_4$ and $LiCoPO_4$ M-O-P bond angles. P3 and P4 have a significant difference in bond angle between the $LiFePO_4$ and $LiCoPO_4$ structure. The structures were obtained from geometry and electronic optimizations in CRYSTAL.[1]

	Bond length (Å)		
Pathway	$LiFePO_4$	$LiCoPO_4$	Difference in Bond lengths
P1	1.57 + 2.226 = 3.796	1.571 + 2.173 = 3.744	(-0.001) + 0.053 = 0.052
P2	1.57 + 2.054 = 3.624	1.571 + 2.053 = 3.624	(-0.001) + 0.001 = 0
P3	1.532 + 2.188 = 3.72	1.534 + 2.113 = 3.647	(-0.002) +0.075 =0.0073
P4	1.553 + 2.098 = 3.651	1.549 + 2.084 = 3.633	0.004 + 0.014 = 0.018

Table 2 Comparison of the $LiFePO_4$ and $LiCoPO_4$ M-O-P bond lengths in the olivine structure. For P1, P3 and P4 $LiCoPO_4$ has shorter bond lengths compared with $LiFePO_4$. The structures were obtained from geometry and electronic optimizations in CRYSTAL.[1]

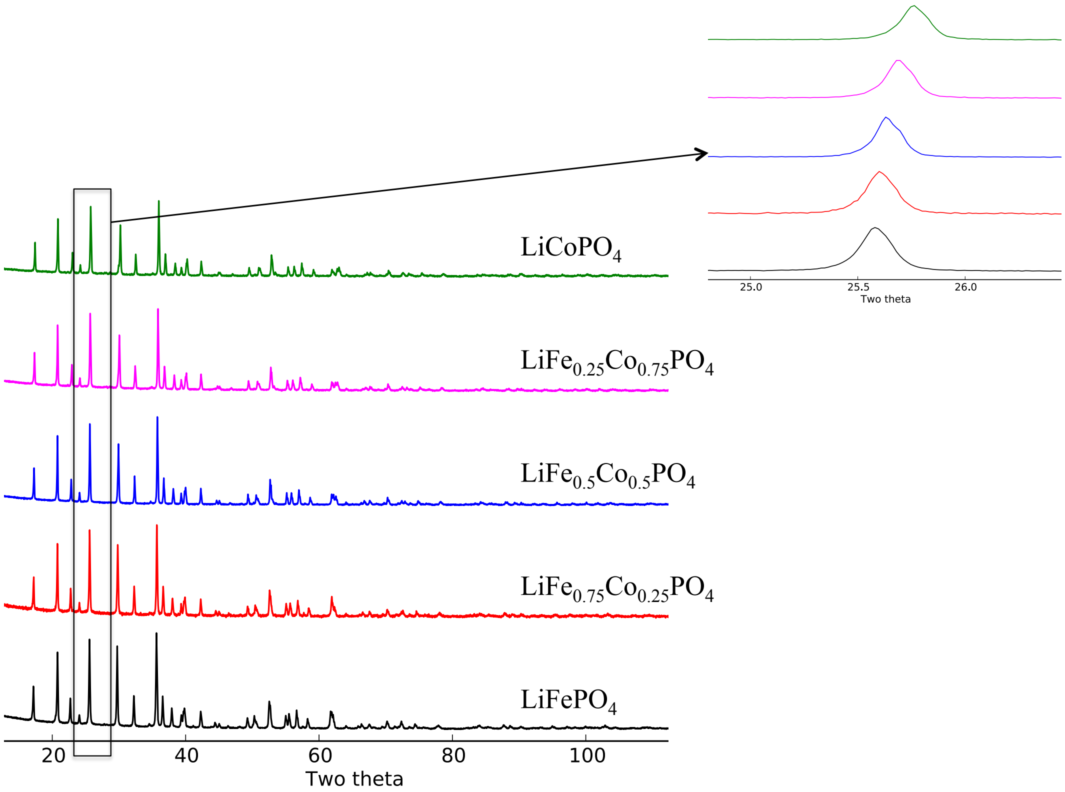

Fig. 2 Overlay of the X-ray diffraction patterns of $LiFe_xCo_{1-x}PO_4$. There is a continual and gradual shift of the peaks to larger 2θ as the Co content increases (inset).

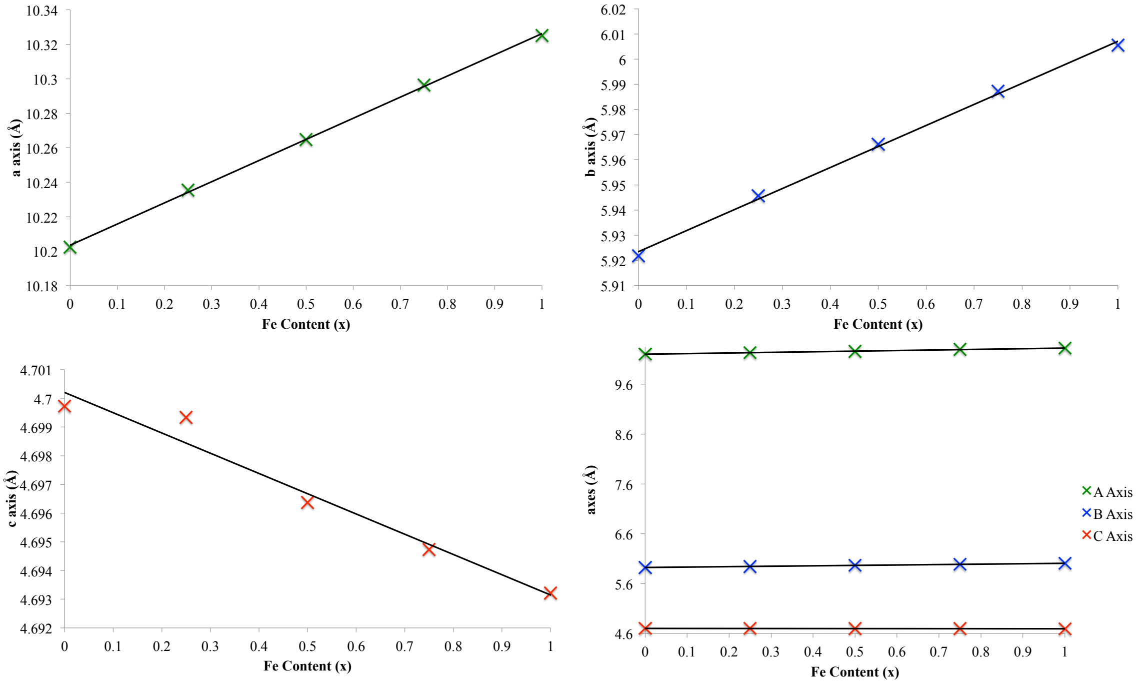

Fig. 3. The affect on the unit cell parameters as calculated from Rietveld refinements as a function of Fe content. There is a linear relationship (R^2 = 0.9995, 0.99806 and 0.96394 for the a, b and c axes, respectively) as the Fe content increases. This is standard Vegard-type behaviour.

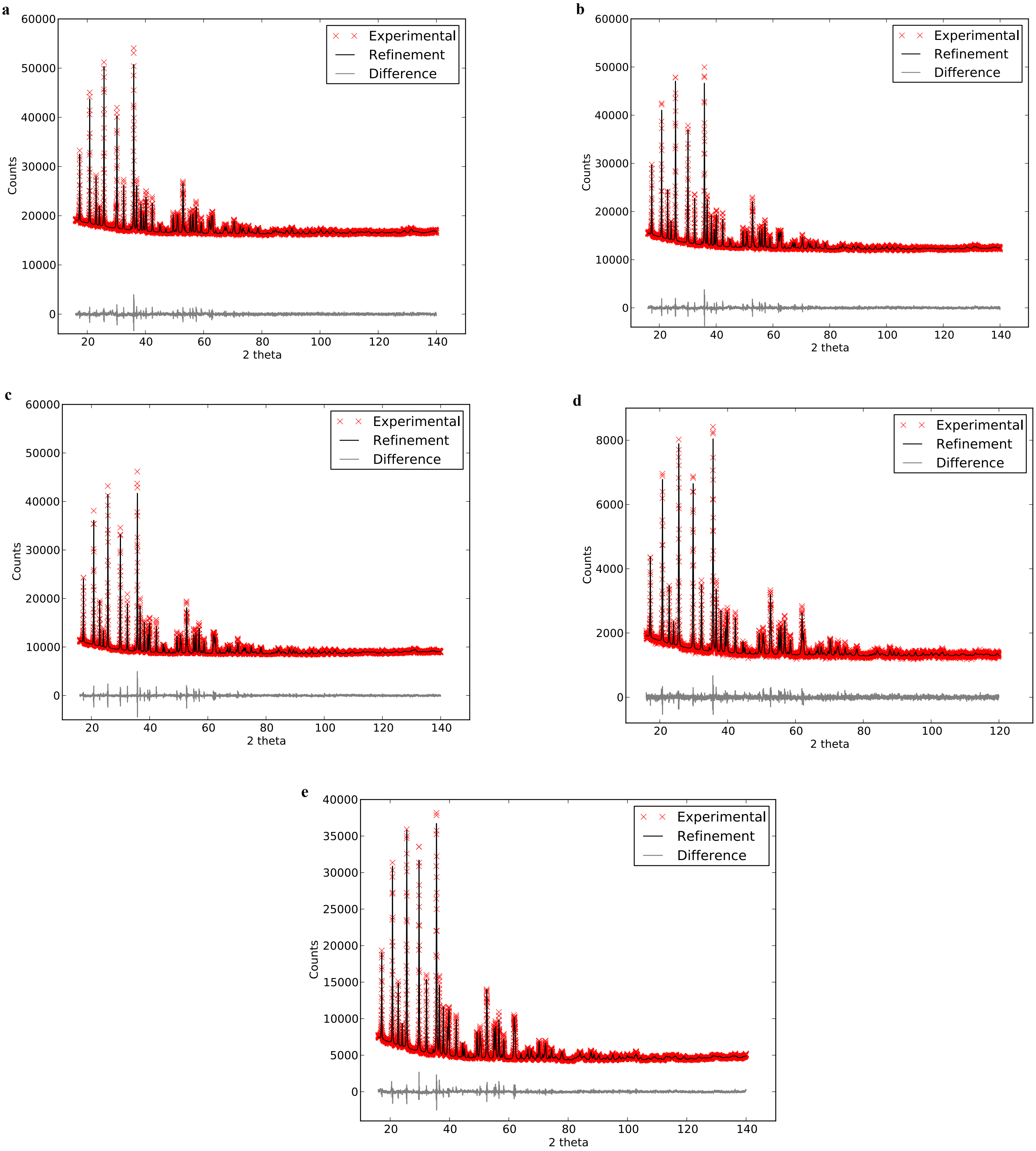

Fig. 4 The X-ray diffraction patterns and refinements of $LiFe_xCo_{1-x}PO_4$ ($x = 0, 0.25, 0.5, 0.75$ and 1 for (a), (b), (c), (d) and (e), respectively) using the TOPAS Academic Rietveld refinement software.[2]

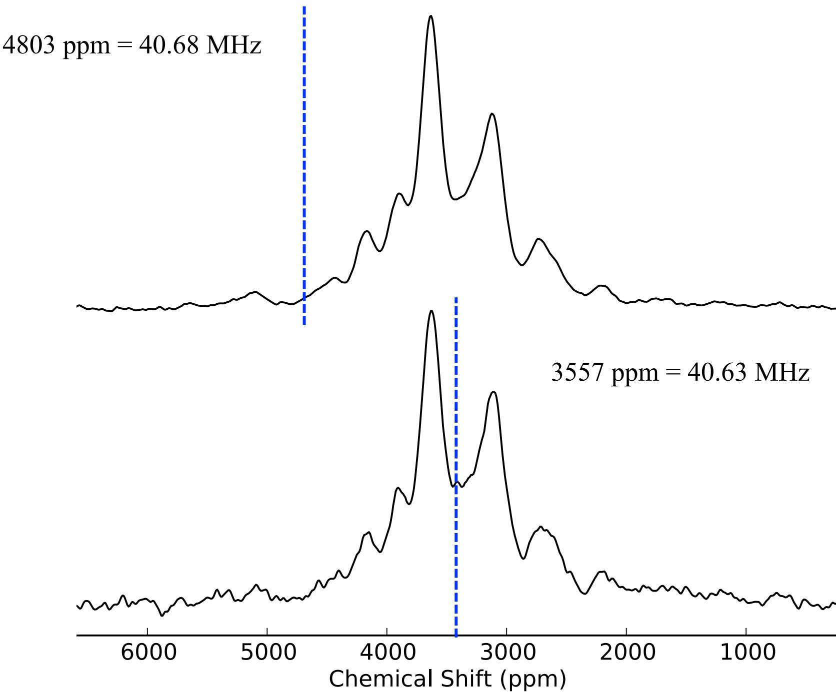

Fig. 5 Two spectra of $LiFe_{0.75}Co_{0.25}PO_4$ collected at a magnetic field of 100 MHz using a Hahn echo pulse sequence using different carrier frequencies. The patterns have had different number of scans (819200 and 51200 in (a) and (b), respectively), resulting in different signal to noise ratio.

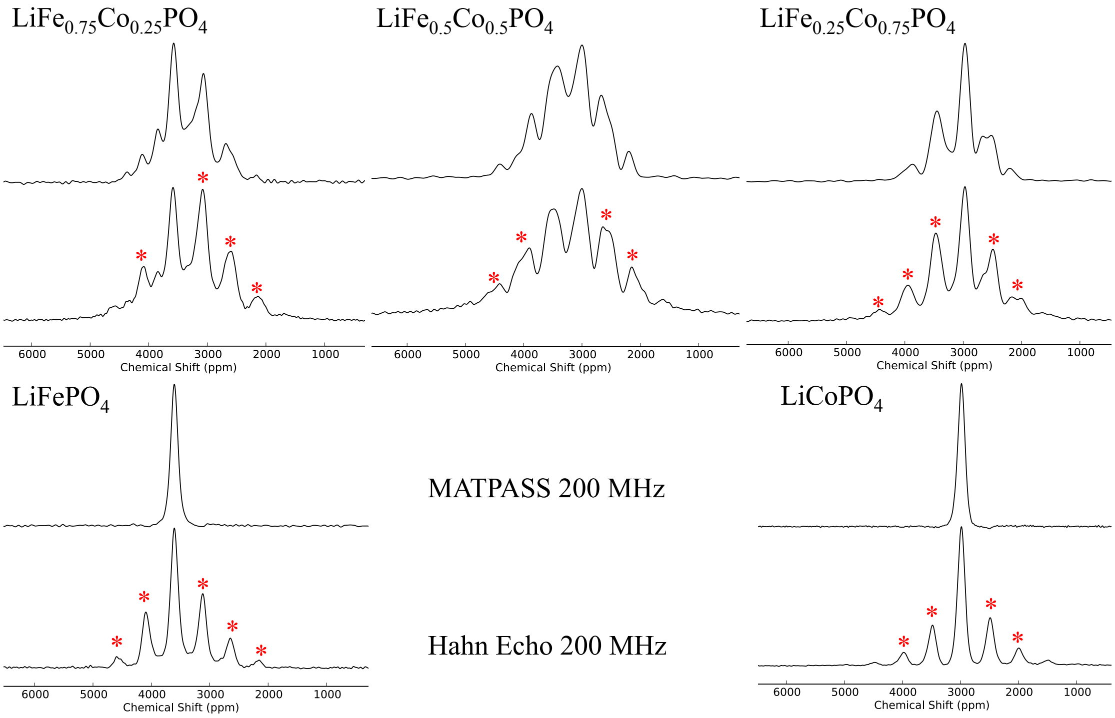

Fig. 6 MATPASS (top spectra) and Hahn Echo (bottom spectra) experiments carried out at a 200 MHz magnetic field and a spinning frequency of 40 kHz.

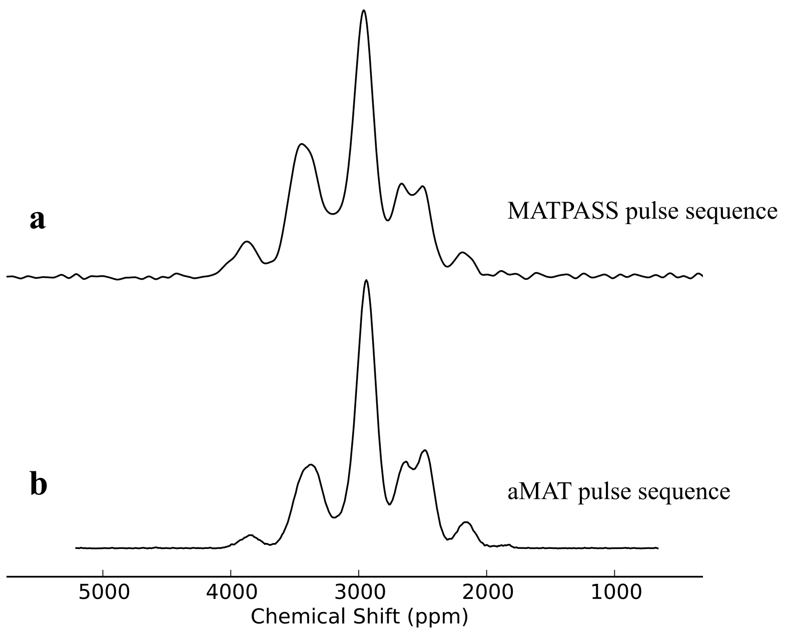

Fig. 7 The ^{31}P MAS spectra of $LiFe_{0.25}Co_{0.75}PO_4$ using the (a) MATPASS and (b) aMAT pulse sequences on the 200 MHz magnet using a spinning frequency of 40 kHz.

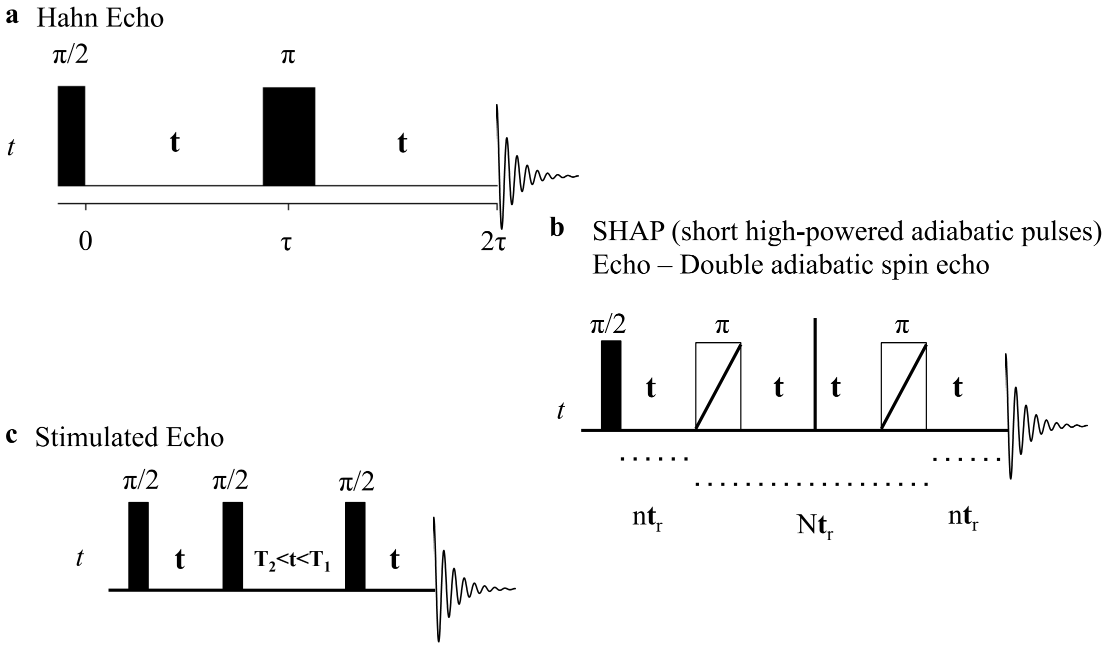
a Hahn Echo

b SHAP (short high-powered adiabatic pulses) Echo – Double adiabatic spin echo

c Stimulated Echo

Fig. 8 The three 1D pulse sequences used to test the excitation window of the radio frequency pulses that are employed in the aMAT and the MATPASS experiments. The (a) Hahn echo was used to make the “model spectrum” for perfect excitation. The (b) SHAP echo[3] consists of adiabatic pulses, like those used in the aMAT and the (c) stimulated echo uses 90° pulses, like the MATPASS. $LiNiPO_4$ resonates at 1800 ppm.

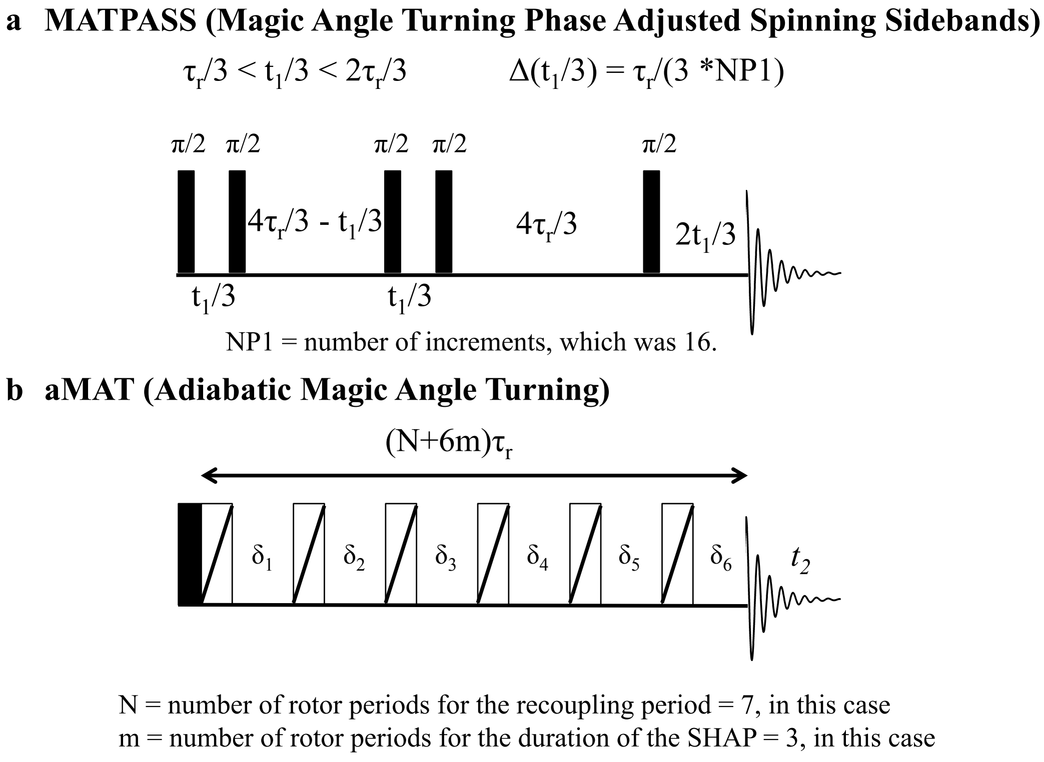

a MATPASS (Magic Angle Turning Phase Adjusted Spinning Sidebands)

$\tau_r/3 < t_1/3 < 2\tau_r/3$ $\Delta(t_1/3) = \tau_r/(3 * NP1)$

NP1 = number of increments, which was 16.

b aMAT (Adiabatic Magic Angle Turning)

N = number of rotor periods for the recoupling period = 7, in this case
m = number of rotor periods for the duration of the SHAP = 3, in this case

Fig. 9 The two 2D pulse sequences used to separate the sidebands from the isotropic resonances. The (a) MATPASS uses a series of 90° pulses, whereas the (b) aMAT employs adiabatic pulses. Figures adapted from Hung *et al.*[4] and Clément *et al.*[5]

$LiNiPO_4$ Synthesis

$LiNiPO_4$ powders were synthesized by a citric acid assisted homogeneous precipitation method. In a typical procedure, 0.02mol citric acid, 0.011mol lithium acetate, 0.01mol nickel acetate and 0.01mol ammonium dihydrogen phosphate were dissolved respectively in 50ml hot water with stirring to get homogeneous solutions. Then the nickel acetate, ammonium dihydrogen phosphate and lithium acetate solution was added successively into the citric acid solution under vigorous stirring. The mixture was then heated at a water bath with a constant temperature of 90 °C under stirring. After heating for about 10 h, greenish yellow colour precipitates were obtained. The precipitates were separated by centrifugation and washed with ethanol and hot water several times. The powders were dried in an oven at 160 °C for 10 h and then calcined at 800 °C for 10 h in a furnace at atmosphere environment.

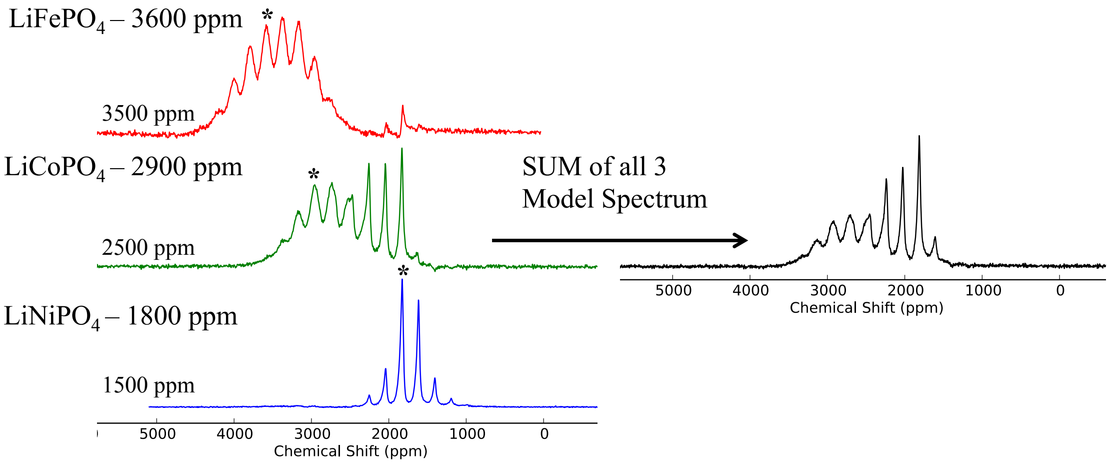

Fig. 10 NMR spectra of a mixture of LiFePO$_4$, LiCoPO$_4$ and LiNiPO$_4$. Hahn echo experiments were recorded at different carrier frequencies (specified on the left) at a 700 MHz magnetic field and then summed as a "model spectrum".

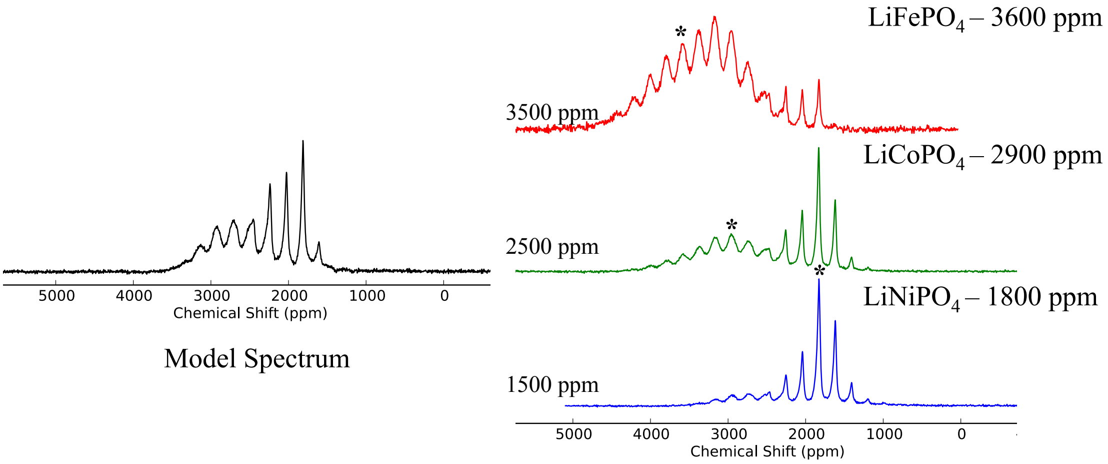

Fig. 11 NMR spectra of a mixture of LiFePO$_4$, LiCoPO$_4$ and LiNiPO$_4$. Stimulated echo experiments were recorded at different carrier frequencies (specified in the middle) at a 700 MHz magnetic field and compared with the model spectrum.

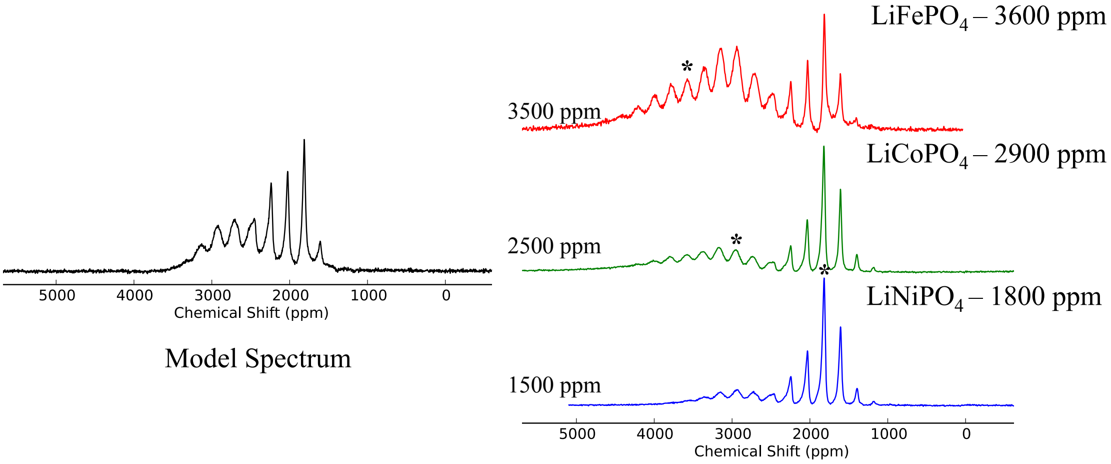

Fig. 12 NMR spectra of a mixture of LiFePO$_4$, LiCoPO$_4$ and LiNiPO$_4$. SHAP echo experiments were recorded at different carrier frequencies (specified in the middle) at a 700 magnetic field and compared with the model spectrum.

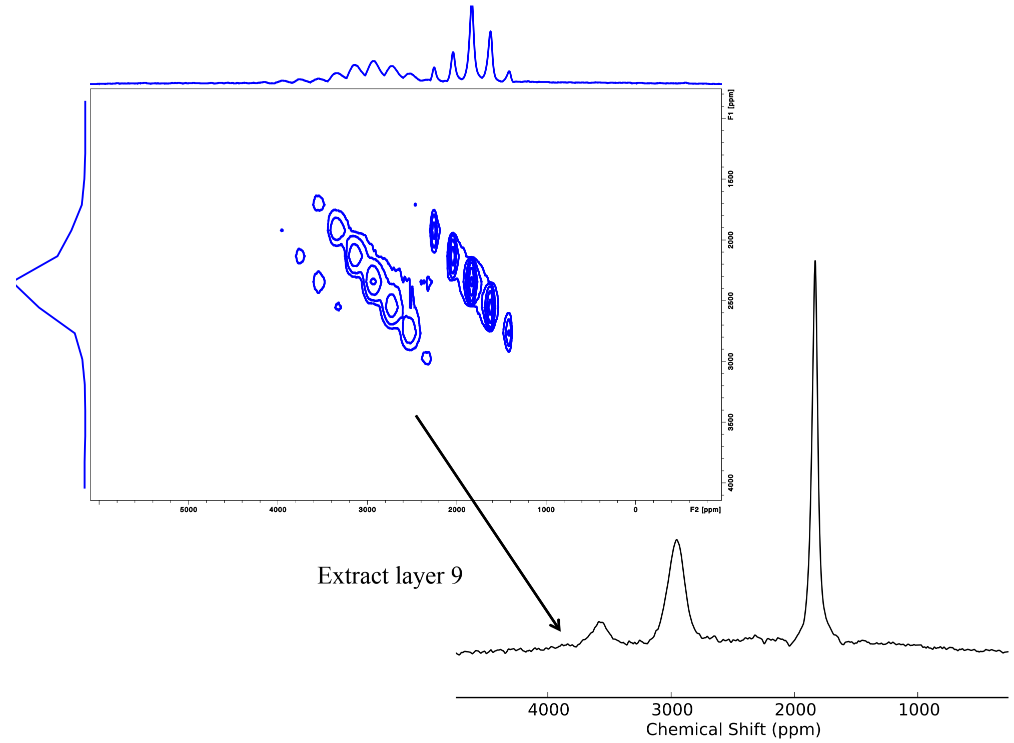

Fig. 13 The MATPASS pulse sequence carried out at a magnetic field of 700 MHz and a spinning speed of 60 kHz on the mixture of $LiNiPO_4$, $LiFePO_4$ and $LiCoPO_4$. This pulse sequence has 16 increments in the indirect dimension. Extracting the 9th layer results in a 1D spectrum of the isotropic peaks.

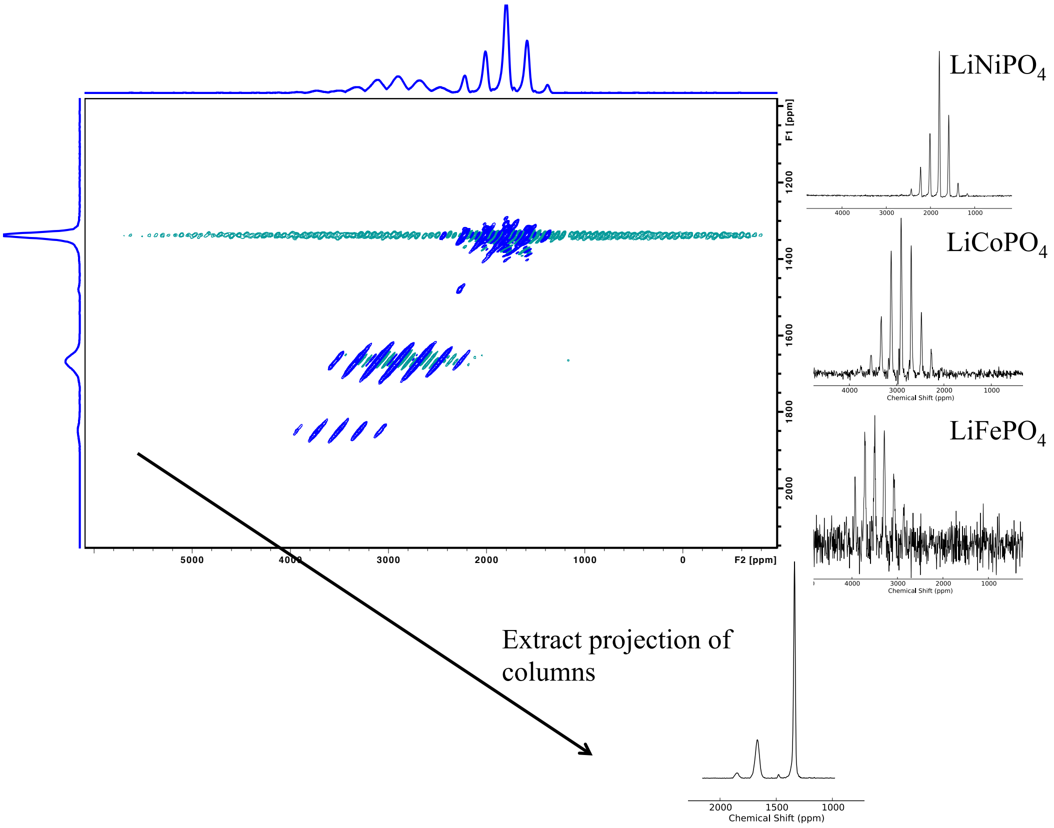

Fig. 14 The aMAT pulse sequence carried out at a magnetic field of 700 MHz and a spinning speed of 60 kHz on the mixture of $LiNiPO_4$, $LiFePO_4$ and $LiCoPO_4$. This pulse sequence has 256 increments in the indirect dimension. The projection in the indirect dimension contains only the isotropic peaks.

	LFP, ppm		LCP, ppm	
	Hyb20	Hyb35	Hyb20	Hyb35
M1	230	201	-436	-412
M2	1925	1629	1344	1142
M3	34	-72	657	517
M4	271	130	271	130
M5 – 2nd Shell	27	-15	-25	12
M6 and M7 – 2nd Shell	-14	-27	7	-9
Sum of moduli	4426	3703	4084	3364
Modulus % from 2nd shell	0.9	1.1	0.8	0.6

Table 3 Contributions of the transition metals in the 2nd coordination shell in $LiMPO_4$ to the P Fermi contact shift. There is less than 2% contribution from the 2nd shell.

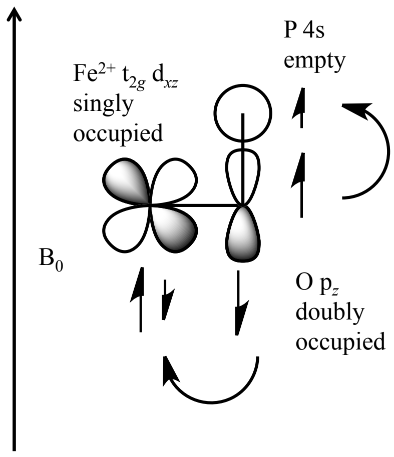

Fig. 15 The electron transfer mechanism (the basis of the Fermi contact shift) for the Fe^{2+}-O-P pathway, which subtends an angle of ~ 90°. The spin density can be transferred onto the empty P 4s orbital via interactions with the Fe^{2+} singly occupied t_{2g} orbital and O p orbital. This results in a positive Fermi contact shift. The mechanism is adapted from Grey *et al.*[6]

Material	Ion	Valence Shell	Size, pm (High-spin octahedral)	Hyb20 δ_{P1}, ppm	Hyb35 δ_{P1}, ppm
$LiMnPO_4$	Mn^{2+}	d^5	97	671	544
$LiFePO_4$	Fe^{2+}	d^6	92	240	20
$LiCoPO_4$	Co^{2+}	d^7	88.5	-436	-412
$MnPO_4$	Mn^{3+}	d^4	78.5	-494	-500
$FePO_4$	Fe^{3+}	d^5	78.5	-752	-785
$CoPO_4$	Co^{3+}	d^6	68.5	-1911	-1935

Table 4 The Fermi contact shift[1] for P1 in six olivine materials. δ_{P1} decreases steadily as the size of the transitional metal ion[7] decreases.

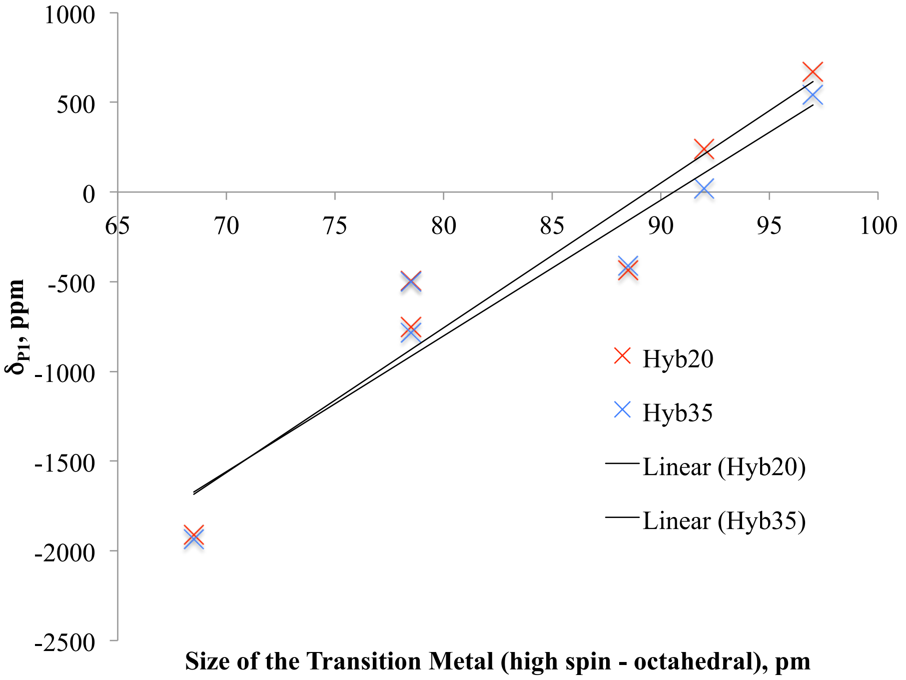

Fig. 16 The relationship between δ_{P1} and the size of the transition metal in the olivine structure for $LiFePO_4$, $LiMnPO_4$, $LiCoPO_4$, $FePO_4$, $MnPO_4$ and $CoPO_4$. There is a linear trend and when the size of the ion is < 90 pm the Fermi contact shift is negative.

P environment	***T_2*' (μs)**
5 Co around P - $LiCoPO_4$	1199
4 Co & 1 Fe	1033
3 Co & 2 Fe	866
2 Co & 3 Fe	700
1 Co & 4 Fe	533
5 Fe around P - $LiFePO_4$	367

Table 5 The T_2' values used for the Fe/Co configurations around P, based on the T_2' values from the end members.

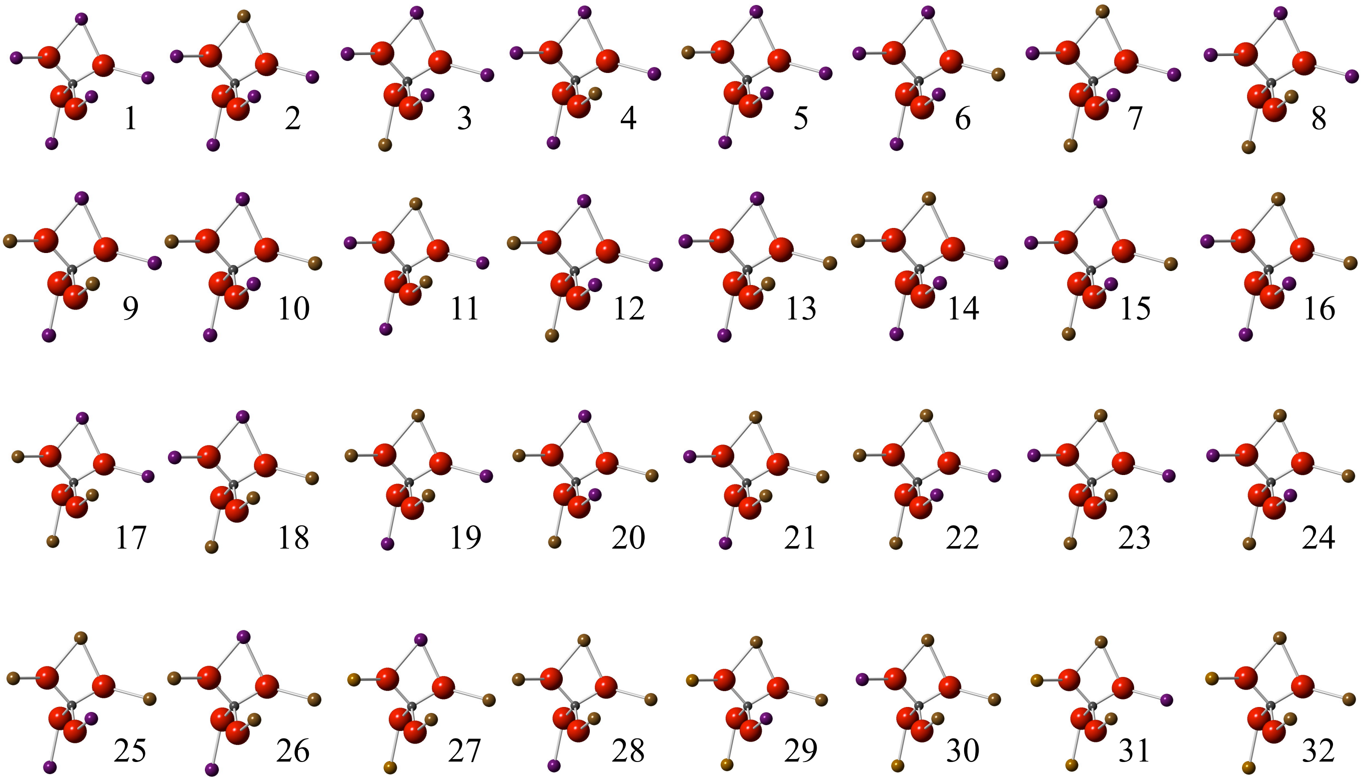

Fig. 17 The 32 possible configurations of Fe and Co around P in the olivine structure, $LiFe_xCo_{1-x}PO_4$ and the associated labels used in the Monte Carlo simulations, Fe is in brown and Co is in purple.

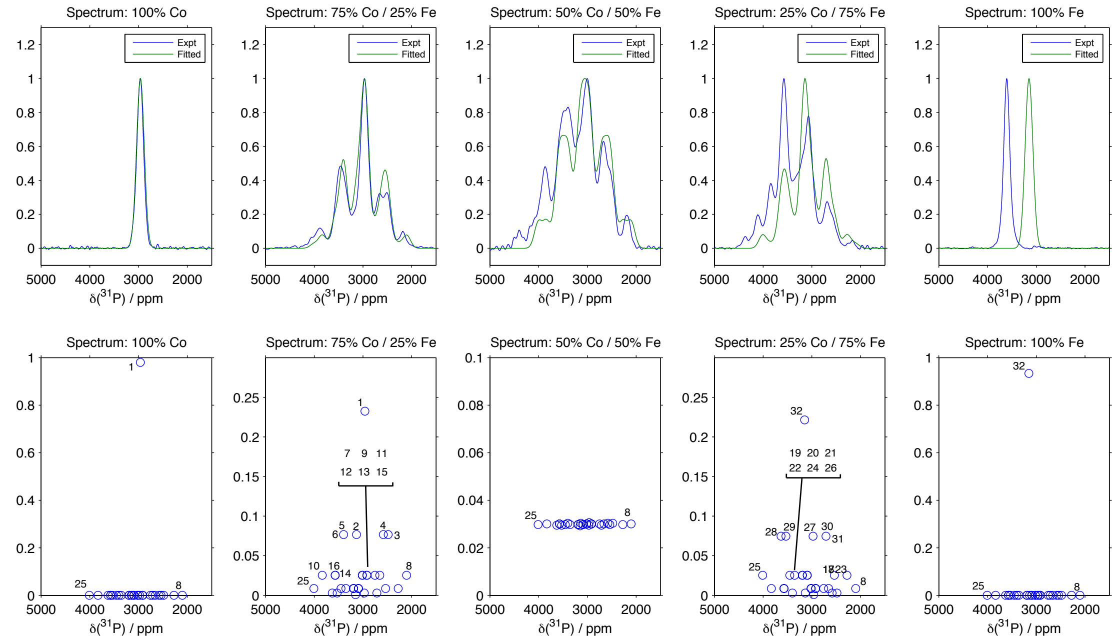

Fig. 18 Monte Carlo fittings of the calculations using all 32 possible Fe/Co configurations around P and fixing them across all 5 spectra, using the Hyb20 calculations as starting values (R^2 = 0.9852, 0.9462, 0.9081, 0.6469 and -1.3938 for $LiFe_xCo_{1-x}PO_4$, where x = 1, 0.75, 0.5, 0.25 and 0, respectively.

References

1 D. S. Middlemiss, A. J. Ilott, R. J. Clément, F. C. Strobridge, and C. P. Grey, *Chem. Mater.*, 2013, **25**, 1723–1734.

2 A. A. Coelho, *Acta Crystallogr A Found Crystallogr*, 2007, **63**, 400–406.

3 G. Kervern, G. Pintacuda, and L. Emsley, *Chemical Physics Letters*, 2007, **435**, 157–162.

4 I. Hung, L. Zhou, F. Pourpoint, C. P. Grey, and Z. Gan, *J. Am. Chem. Soc.*, 2012, **134**, 1898–1901.

5 R. J. Clément, A. J. Pell, D. S. Middlemiss, F. C. Strobridge, J. K. Miller, M. S. Whittingham, L. Emsley, C. P. Grey, and G. Pintacuda, *J. Am. Chem. Soc.*, 2012, **134**, 17178–17185.

6 C. P. Grey and N. Dupré, *Chem. Rev.*, 2004, **104**, 4493–4512.

7 R. D. Shannon, *Acta Crystallogr A Found Crystallogr*, 1976, **A32**, 751–767.